Hubbard Model Simulation Using Multi-mode cavity coupled to qubits

Guo (Jerry) Zheng
Department of Physics, University of Oxford

Supervisor: Steven Girvin
Department of Physics, Yale University

(Dated: August 28, 2020)

We simulate the one dimensional Hubbard model using multiple cavities, each coupled to a transmon qubit in the dispersive regime, along with a set of controls such as beam splitters and two-mode squeezers. With an improved implementation of GRAPE algorithm from QuTip, we demonstrate an infidelity of around 99.9% for dynamics simulation of one spin-up electron and one spin-down electron on four sites with weak nearest-neighbor interaction. The ground state of the model can also be approximated from variational method via GRAPE algorithm. The variational ground state of the half-filled Hubbard model reaches an overlap of 99% with the ground state from diagonalization.

I. INTRODUCTION

Traditionally, the fundamental bits of quantum computing has been discrete two-level qubits. In order to encode quantum information into the discrete qubits, a large number of qubits are needed, which imposes threat from the decoherence errors and other experimental constraints. Another popular proposal has been encoding the information in continuous variable qubits, also known as bosonic qubits, such as stationary modes in a cavity. In particular, the information can be encoded in a superposition of coherent states called cat states [1] or other propositions like the GKP states [2].

Since the harmonic oscillators has degenerate transition energies, quantum control is relatively difficult compared to traidtional qubits. Law and Eberly [3] has shown that when a qubit and an oscillator in resonance are coupled together, the added non-linear control enables universal control on the oscillator. Since there are certain experimental advantages in operating under the far off-resonant condition, further work has been done to demonstrate universal controls on states preparations [4] and simulating non-trivial operations [5].

One-dimensional Hubbard model is a simple yet fundamental model in condensed matter physics that reveals underlying mechanisms of many complicated phenomena. In our work, we aim to simulate the 1D Hubbard model with multiple cavities, each coupled to a transmon qubit, with a set of controls on the cavity-qubit system and also between the cavities, such as beam splitters and two-mode squeezers. In particular, we have modified QuTip's implementation [6] of GRAPE algorithm for optimal control to simulate the dy-

namics and perform variational method. The modifications improved the infidelity from less than 90% to 99.9% for simulating the dynamics of one spin-up electron and one spin-down electron on 4 sites when the nearest-neighbor interaction is weak. For half-filled Hubbard model, the variational ground state has an overlap of 99% with the ground state from diagonalization.

II. THEORY

A. Hubbard model

The one dimensional Hubbard model is an extension of the tight-binding model with the addition of the electron-electron repulsion U. The Hamiltonian is expressed as

$$\hat{H} = \hat{T} + \hat{V},$$

where

$$\hat{T} = -t \sum_{i,\sigma} \left(\hat{c}^{\dagger}_{i,\sigma} \hat{c}_{i+1,\sigma} + \hat{c}^{\dagger}_{i+1,\sigma} \hat{c}_{i,\sigma} \right)$$

and

$$\hat{V} = U \sum_{i} \hat{n}_{i,\uparrow} \hat{n}_{i,\downarrow}.$$

Here, $\hat{T}$ is the hopping Hamiltonian, $\hat{V}$ is the nearest-neighbor interaction, and $\hat{c}_{i,\sigma}$ is the fermion annhilation operator for electrons of spin $\sigma = \uparrow$ or $\downarrow$ on site i. With the introduction of periodic boundary conditions, the hopping Hamiltonian includes hopping between the last sit and the first site and vice versa. Since there is no spin-flipping mechanism in this simplification, electrons of different spin flavors can be viewed as distinguishable particles.

Taking into consideration of the Pauli exclusion principle, when there are N_{up} and N_{down} number of spin-up and spin-down electrons respectively on N_{site} sites, the Hilbert space dimension increases as

$$N_{dim} = \dim\left(H_{up}\right) \times \dim\left(H_{down}\right) = \binom{N_{site}}{N_{up}} \times \binom{N_{site}}{N_{down}}.$$

The Hilbert space dimension increases rapidly. In our work, the largest Hilbert space is reached when there are 2 spin-up and 2 spin-down electrons on 4 sites, in which case the dimension is $6 \times 6 = 36$. Worth noting that when dealing with simulations in cavity-qubit systems, the need of some auxiliary cavity levels and the existence of the two-level qubits also boosts the dimension of the unitary in computation. As an example, when simulation the 2 spin-up and 2 spin-down electrons case, the truncated Hilbert space needs at least 16 cavity levels according to Appendix C. Then, the resulting unitary has a dimension of $(16 \times 2)^2 = 1024$, which is prohibitive in computational power especially when parallel computing and GPU are not applied yet.

B. Cavity-qubit coupling

Consider the far off-resonant case, where the Jaynes-Cunnings interaction is reduced to the dispersive Hamiltonian

$$\hat{H}_d = \chi \hat{a}^\dagger \hat{a} |e\rangle\langle e|. \tag{1}$$

Adopting the experimental value from to Ref. [5], $\chi/2\pi = -2.2MHz$. This dispersive Hamiltonian is also called the drift Hamilonian in the context of optimal control. χ is an important measure of the capability of control. The time allowed for the control pulse should be at least in the order of $2\pi/\chi$ for universal control[7]. Note that decoherence errors, such as damping, and Kerr non-linearity are not included in the simulations for now because simulating open systems requires driving the density matrix or superoperators under the Lindblad master equation. The controls are the drive Hamilonian applied on the cavity and the transmon

$$\hat{H}_c = \epsilon_c \hat{a} + \epsilon_T \sigma_- + h.c.,$$

where ϵ_c and ϵ_T are complex numbers. Since GRAPE algroithm only optimizes real control amplitudes, the set of controls are expressed as $\left\{\hat{a} + \hat{a}^\dagger, i\left(\hat{a} - \hat{a}^\dagger\right), \sigma_x, \sigma_y\right\}$ where the control amplitudes serve as the real and imaginary parts of ϵ_c and ϵ_T.

When two cavities each coupled to a qubit are in use, the Hilbert space is $\hat{H} = \hat{H}_1 \otimes \hat{H}_2$. Besides having independent controls on each cavity as before, the cavities need to interact to form entangled states to simulate the nearest-neighbor interaction of the Hubbard model. Thus, the beam splitter and two-mode squeezing controls are introduced, which have expressions $\left\{\hat{a}_1^\dagger \hat{a}_2 + \hat{a}_1 \hat{a}_2^\dagger, i\left(\hat{a}_1^\dagger \hat{a}_2 - \hat{a}_1 \hat{a}_2^\dagger\right)\right\}$ and $\left\{\hat{a}_1^\dagger \hat{a}_2^\dagger + \hat{a}_1 \hat{a}_2, i\left(\hat{a}_1^\dagger \hat{a}_2^\dagger - \hat{a}_1 \hat{a}_2\right)\right\}$ respectively. Note that $\hat{a}_1$ and $\hat{a}_2$ are the annihilation operators on cavity 1 and 2.

Symmetric spin configurations

Some important simplifications can be introduced from symmetry when the number of spin-up and spin-down electrons are equal. Since the Hubbard Hamiltonian and the electron spin configurations are both exchange symmetric with respect to spin-flavor exchange, the controls applied to the two cavities should also be identical. Thus, the controls can be reduced to a set of symmetric controls on both cavities $\left(\hat{a}_1 + \hat{a}_1^\dagger + \hat{a}_2 + \hat{a}_2^\dagger\right)$, $\left[i\left(\hat{a}_2 - \hat{a}_2^\dagger\right) + i\left(\hat{a}_1 - \hat{a}_1^\dagger\right)\right]$, $\left(\sigma_{1,x} + \sigma_{2,x}\right)$, and $\left(\sigma_{1,y} + \sigma_{2,y}\right)$.

Note that while both terms of the two-mode squeezer control are symmetric, the second term of the beam splitter control is anti-symmetric, so it mush vanish. As a result, the symmetric beam splitter control is only left with $\left(\hat{a}_1^\dagger \hat{a}_2 + \hat{a}_1 \hat{a}_2^\dagger\right)$. A summary of the possible types of controls is included in Table I.

C. Encoding from site basis to cavity level basis

The encoding maps energy levels of the cavity with the qubit in the ground state to the site basis representing which sites are occupied by electrons. For the ease of generalization, we have chosen the encoding that each cavity-qubit system encodes the electron state of each spin-flavor. For example, assume one of the cavity encodes the spin-up electrons' state. Then when there are one spin-up electron, the chosen encoding maps the site basis $\begin{pmatrix} \hat{c}_1^\dagger|0\rangle \\ \hat{c}_2^\dagger|0\rangle \\ \hat{c}_3^\dagger|0\rangle \\ \hat{c}_4^\dagger|0\rangle \end{pmatrix}$ to the cavity-qubit levels $|n, g\rangle$ where n = 1,2,3,4. Similarly, when there are two electrons, the chosen encoding maps the site basis $\begin{pmatrix} \hat{c}_2^\dagger\hat{c}_1^\dagger|0\rangle \\ \hat{c}_4^\dagger\hat{c}_1^\dagger|0\rangle \\ \hat{c}_3^\dagger\hat{c}_1^\dagger|0\rangle \\ \hat{c}_4^\dagger\hat{c}_2^\dagger|0\rangle \\ \hat{c}_3^\dagger\hat{c}_2^\dagger|0\rangle \\ \hat{c}_4^\dagger\hat{c}_3^\dagger|0\rangle \end{pmatrix}$ to the first 6 cavity levels. We have found that the infidelity of dynamics simulation deteriorates when the fock state transfer is far. Thus, the encodings are chosen such that the non-zero elements of the hopping Hamiltonian expressed in the cavity level basis are relatively close to the diagonal to reduce the number of far Fock state transfers.

With the encoding specified, the Hubbard Hamiltonian $\hat{H}$ can be mapped to the cavity basis. Note that for practical reasons, the Hubbard Hamiltonian is expected to be simulated by the cavity when the qubit starts and ends in ground state. Therefore, the mapped Hamiltonian comes with the ground state projector $|g\rangle\langle g|$. Explicit expressions of the matrix entries are shown in Appendix B 1.

When the encoding is extended to two cavities, it can be easily generalized assuming the encoding to be identical for both. As an example, the state in the site basis $\left(\hat{c}_{\uparrow,2}^\dagger \hat{c}_{\uparrow,1}^\dagger \hat{c}_{\downarrow,2}^\dagger \hat{c}_{\downarrow,1}^\dagger\right)|-,-,-,-\rangle = |\uparrow\downarrow,\uparrow\downarrow,-,-\rangle$ maps to the cavity ground state of $|0, g\rangle \otimes |0, g\rangle$.

III. MODIFIED GRAPE ALGORITHM

GRAPE algorithm is one of the leading optimal control algorithms that are gradient-based. It performs optimization on the control amplitudes to minimize the cost function. The algorithm divides the control pulses to piece-wise constant controls. In our project, we have used QuTip's implementation of GRAPE. QuTip's implementation is advantageous since it adopts the classic FORTRAN implementation of the quasi-Newton L-BFGS-B optimization method, to optimize the control pulses so it is much faster and normally guarantees monotonic convergence. However, QuTip's implementation is not very flexible. For example, it does not offer customized fidelity/cost function and manually input initial control amplitudes. Detailed modifications can be seen in Appendix D.

In particular, GRAPE is used in our project for two purposes: simulating the unitary dynamics and finding the ground state via variational method.

A. Dynamics simulation

Dynamics simulations attempts to reconstruct the unitary driven by the Hubbard Hamiltonian with the unitary driven by the control pulses. The fidelity is based on the Hilbert-Schmidt inner product between the target and pulse-driven unitary. Modifications are introduced for our specific problem because of two reasons.

1. The truncated Hilbert space dimension N_{cav} is larger than the effective Hilbert space dimension N_{dim}. In fact, the auxiliary cavity energy levels outside of the effective levels are expected to have non-zero amplitude only during the control pulse sequence, but vanish at the end of the control pulse sequence.

2. The unitary driven by the Hubbard Hamiltonian is defined to be encoded in the states where the qubit starts and ends in the ground state.

To conclude, the effective space in the cavity-qubit space are states occupying the first N_{dim} cavity levels when the qubit is in the ground state. The fidelity expression should only take into consideration of the unitary that stays within the effective space. The modified expression is then

$$\text{infidelity} = 1 - \frac{\left| Tr\left\{ \hat{I}_{N_{dim},gg} \left(\hat{U}_{targ}^{-1} \hat{U}_{pulse} \right) \right\} \right|}{N_{dim}}, \text{ where } \hat{I}_{N_{dim},gg} = \left[\begin{array}{c|c} \hat{I} & \\ \hline & \mathbf{0} \end{array} \right] |g\rangle\langle g|$$

Not here $\left[\begin{array}{c|c} \hat{I} & \\ \hline & \mathbf{0} \end{array} \right]$ is a $N_{cav} \times N_{cav}$ matrix with the identity matrix $\hat{I}$ of size $N_{dim} \times N_{dim}$. Similar expressions can easily be extended to the double cavity expressions.

This modification is critical for improving the performance of GRAPE since it focuses more on where the core information is at. As an example, when simulating one electron hopping on four sites, the fidelity can increases from 90% to 99.999% after making this modification.

GRAPE algorithm requires the input of the physical parameters and some parameters for optimization. In particular, the choice of Hilbert space truncation dimension and the number of time slices can be affect the performance and accuracy of GRAPE. Thus, it is advantageous to choose values that enable decent performance but also do not take up too much computational power.

B. Variational method

For variational method, the modifications are on the Hubbard Hamiltonian. Since the Hubbard Hamiltonian is only defined for the effective Hilbert space within the first N_{dim} levels of the cavity when the qubit is in ground state, ground states of the cavity-qubit system can have lower energy than the physically allowed one(s) when there are more than one cavity used or the ground state energy of the physical system is higher than zero.

For example, when the electrons are strongly correlated and the Hubbard model is half-filled, i.e. $U \gg t$, in the ground state there should be no site occupied by both a spin-up and a spin-down electron and the ground state energy should be of order t^2/U as derived in Appendix B 2. However, the ground state of the cavity-qubit system can be one cavity occupying an auxiliary level and the other being in the ground state of the hopping Hamiltonian without the penalty of nearest-neighbor interactions since the cavity in the auxiliary level do not have a physical mapping to the site basis.

In order to fix this issue, a penalty Hamiltonian can be added on the auxiliary levels. The infidelity (cost function) expression to be minimized is then

$$\text{infidelity} = \langle f|\hat{H}'|f\rangle = \langle i|\hat{U}^{\dagger}_{pulse}\hat{H}'\hat{U}_{pulse}|i\rangle,$$

where $\hat{H}' = \hat{H} + \hat{H}_{penalty}$ and

$$\hat{H}_{penalty} = p\sum_i \left(|i\rangle\langle i| \otimes \hat{I} + \hat{I} \otimes |i\rangle\langle i|\right), \text{where } |i\rangle \text{ are the auxiliary levels.}$$

p is the penalty Hamiltonian magnitude and should be set to a positive value much larger than the estimated ground state energy.

C. Initial state choice

As noted in Section II B, there are some simplifications introduced for the control types from the exchange symmetry between the spin-up and spin-down electrons. While that works for dynamics simulation naturally, it is not so trivial in variational method.

The Hubbard Hamiltonian commutes with the exchange operator

$$\left[\hat{H}, \hat{P}_{\uparrow,\downarrow}\right] = 0,$$

so each eigenstate of the Hubbard Hamiltonian have definite eigenvalues for the exchange operator, i.e. ± 1. The control pulses, as demonstrated before, are exchange symmetric, therefore the final state evolved from the pulse-driven unitary only finds the lowest energy eigenstate of the Hubbard Hamiltonian with the same exchange symmetry or anti-symmetry as the initial state. Thus, assuming the ground state is non-degenerate, the variational method needs to be performed for both symmetric and anti-symmetric initial states to determine which final state reached has lower energy expectation.

IV. DYNAMICS SIMULATION RESULTS

Without specification, the hopping magnitude is set to $t = \chi/40 = 2\pi \times 0.055$MHz and the control pulse length to $\tau = 10.0\mu s$ to have the dynamics evolve though a non-trivial phase of around π. Note that t/χ can be set to as low as 4 for simulating 2 spin-up electrons case while maintaining a performance of 99.95%. Having low t/χ ratio is beneficial for reducing the decoherence errors. Here the choice of 40 is more of a safety one considering the introduction of nearest-neighbor interaction when both spins are present.

According to Appendix C, the parameters of GRAPE algroithms are chosen to be $N_{cav} = 10$ and $N_{ts} = 40$ for cavities simulating 1 spin-up electron and $N_{cav} = 16$ and $N_{ts} = 60$ for cavities simulating 2 spin-up electrons.

A. Electrons with the same spin flavors

It is in general much easier to simulate electrons with only the same spin flavors with single cavity since there is no nearest-neighboring interaction involved. The results of simulating spin configurations [1,0] and [2,0] are shown in Figure 1. The worsen in the infidelity from one to two electrons is likely because the increase in effective Hilbert space dimension requires more control of the higher cavity levels.

Still, the infidelity is decent as it approaches 99.999% for single spin-up electrons and 99.9% for two spin-up electrons. Note that three spin-up electron case is not included since it is essentially having one hole and has the same hopping Hamiltonian as one electron case does.

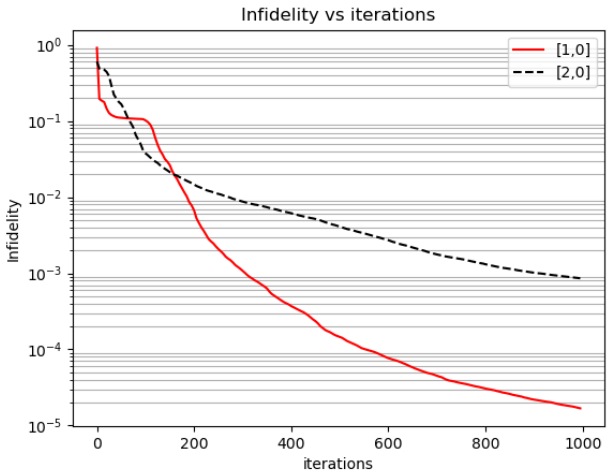

FIG. 1: Infidelity vs GRAPE iterations for dynamics simulation. The label shows the spin configurations $[N_{up}, N_{down}]$

B. Electrons with both spin flavors

With reasons stated in Section II A, [1,1] is the largest Hilbert space that can be simulated with the current computation power we have.

According to the model selection procedure described in Appendix C, adopt the control type of having identical controls on the two cavities with symmetric beam splitter controls. A direct comparison of the performance under different U/t ratios is shown in Figure 2.

Through mapping the probability densities of the effective cavity levels to the sites, the electron densities can be plotted for both the target dynamics evolution and the pulse-driven evolution. Figure 3 provides a comparison between the Hamiltonian-driven dynamics and the pulse-driven dynamics. Here, each pulse sequence is of length $2\mu s$ and is applied 5 times repeatedly. The two matches very well at the end of each pulse sequence as expected.

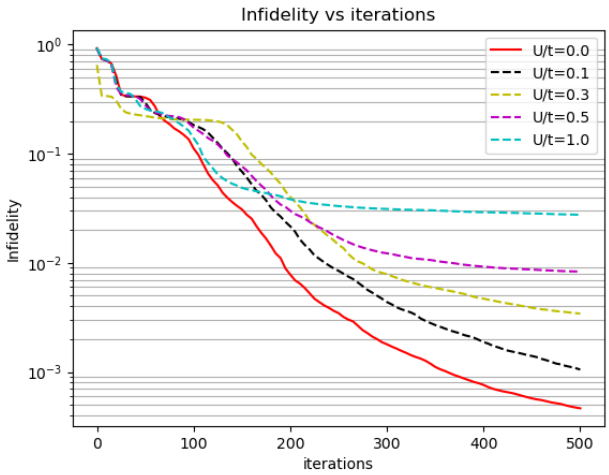

FIG. 2: Infidelity of dynamics simulation for [1,1] vs GRAPE iterations with identical quadrature controls and symmetric beam splitter controls.

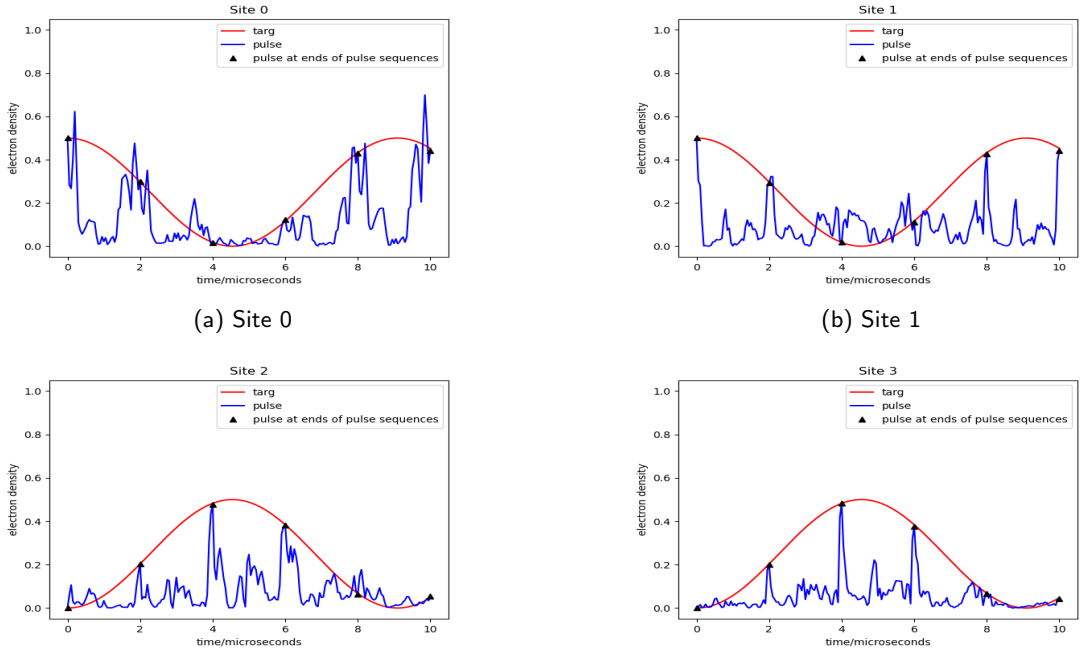

(a) Site 0

(b) Site 1

(c) Site 2

(d) Site 3

FIG. 3: Spin down electron density evolution comparison between Hamiltonian-driven and pulse-driven dynamics. The pulse-driven values at the end of each pulse sequence is labeled with black triangles.

V. VARIATIONAL METHOD RESULTS

Compared to dynamics simulation, variational method can be more accessible since it requires much less computation power. According to Appendix C, the parameters are chosen to be be $N_{cav} = 8$ and $N_{ts} = 40$ for cavities simulating 1 spin-up electron and $N_{cav} = 10$ and $N_{ts} = 60$ for cavities simulating 2 spin-up electrons. As derived in Appendix B 2, ground states of the cases of interest are all exchange symmetric or have degenerate ground states. Thus, the initial states are chosen to be exchange symmetric as well. When there are one or two electrons of the same spin, i.e. [1,0] or [2,0], the comparison is shown in Figure 4. The performance of the variational method for single spin flavor is extremely well. It reaches the ground state energy with errors of order 10^{-4} to 10^{-5}.

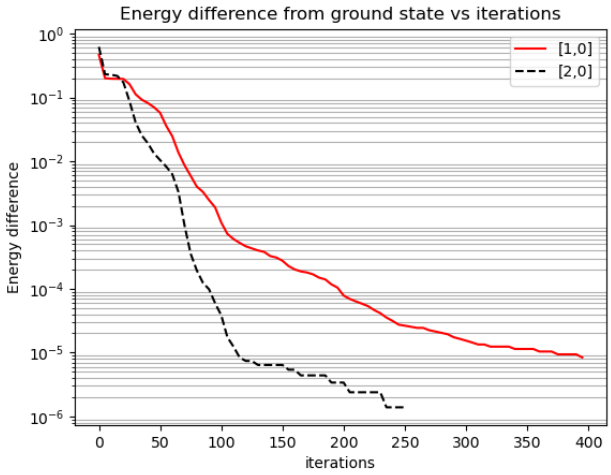

FIG. 4: Absolute energy difference compared to ground state energy vs GRAPE iterations for variational method. The label shows the spin configurations $[N_{up}, N_{down}]$

With a similar procedure to dynamics simulation, it is found that when both spin flavors are included, having identical quadrature controls and two-mode squeezer controls can have the best performance. A comparison of variational method performance on 2 spin-up and 2 spin-down electrons is shown in Figure 5.

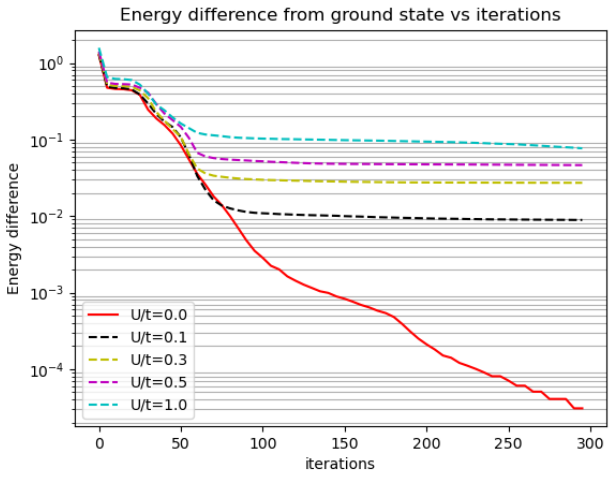

FIG. 5: Absolute energy difference compared to ground state energy vs GRAPE iterations for variational method with identical quadrature controls and two-mode squeezer controls.

VI. OTHER ATTEMPTS

a. Adiabatic method With the modifications specified in Appendix D 2 b, we are able to have arbitrary input pulse values. One attempts we were able to make is to first optimize the pulse under the condition that nearest-neighbor interaction U = 0, and then adiabatically invoke U to the target value while optimizing the control pulses. We hope to avoid any traps by doing so. However, the improvement from applying adiabatic method is not significant by far.

VII. FUTURE WORK

a. "Ymon" Instead of the current scheme where each cavity is coupled to an independent transmon qubit, it is possible to use a transmon coupled simultaneously to both cavities. This provides stronger interactions that can entangle the two cavities compared to the current scheme.

b. Open system and other constraints Currently, the system is assumed to be a closed system, i.e. not including any decoherence errors, since it costs much more computation power to simulate open systems. Moreover, there should be constraints imposed on the control pulses, such as its amplitude and frequency, but QuTip do not support this function for now.

c. Generalization In order to generalize the Hubbard Model to more sites and including any number of electrons, commutation relation of fermion operators needs to be implemented. Some existing library such as OpenFermion and SymPy should be able to achieve that generalization.

VIII. CONCLUSION

In this work, we have simulated one dimensional Hubbard model to a decent standard. With multiple cavities coupled to qubits, different control types' performances are compared and certain symmetry properties are discovered. Particularly, when the nearest-neighbor interaction is weak, the fidelity for dynamics simulation and variational method reaches 99.9% and 99% respectively. However, difficulty still remains in improving the fidelity when the nearest-neighboring interaction is strong. Some possible next steps, such as adopting intra-connected transmon qubits, are proposed to tackle on this problem.

[1] M. Mirrahimi *et al.*, New J. Phys. **16**, 045014 (2014).
[2] D. Gottesman, A. Kitaev, and J. Preskill, Phys. Rev. A **64**, 012310 (2001).
[3] C. K. Law and J. H. Eberly, Phys. Rev. Lett. **76**, 1055 (1996).
[4] R. W. Heeres, B. Vlastakis, E. Holland, S. Krastanov, V. V. Albert, L. Frunzio, L. Jiang, and R. J. Schoelkopf, Phys. Rev. Lett. **115**, 137002 (2015).
[5] R. Heeres *et al.*, Nature Communications **8**, 94 (2017).
[6] J. Johansson, P. Nation, and F. Nori, Computer Physics Communications **184**, 1234 (2013).
[7] S. Krastanov, V. V. Albert, C. Shen, C.-L. Zou, R. W. Heeres, B. Vlastakis, R. J. Schoelkopf, and L. Jiang, Phys. Rev. A **92**, 040303 (2015).
[8] M. H. Goerz, D. Basilewitsch, F. Gago-Encinas, M. G. Krauss, K. P. Horn, D. M. Reich, and C. P. Koch, SciPost Phys. **7**, 80 (2019).

Appendix A: State-to-state transfer

1. Generation of the displacement operator

The displacement operator is defined as $\hat{D}(\alpha) = e^{\alpha\hat{a}^\dagger - \alpha^*\hat{a}}$, and it can be used to generate a coherent state in an oscillator from vacuum. The following is a proof of generating the displacement operator from a perturbation Hamiltonian $\hat{V}(t)$ on the $\hat{q}$ quadrature.

$$\hat{H}_0 = \hbar\omega_R\hat{a}^\dagger\hat{a} \text{ and } \hat{V}(t) = \epsilon\cos\omega_d t\left(\hat{a}^\dagger + \hat{a}\right)$$

The perturbation Hamiltonian in the inetraction picture is expressed as

$$\hat{V}_I(t) = \hat{U}_I\hat{V}(t)\hat{U}_I^\dagger = \epsilon\cos\omega_d t\left(e^{-i\omega_R t}\hat{a}^\dagger + e^{i\omega_R t}\hat{a}\right)$$

Assume the state Ψ evolves with $\hat{T}$, i.e. $i\hbar\frac{\partial}{\partial t}\hat{T}(0,t) = \hat{V}_I(t)\hat{T}(0,t)$. The solution to $\hat{T}$ can be solved iteratively as

$$\hat{T}(0,t) = \Gamma\left\{\exp\left\{-\frac{i}{\hbar}\int_0^t \hat{V}_I(t')dt'\right\}\right\},$$

where $\Gamma\{\cdot\}$ is defined as the Dyson Time-ordering operator. Notice that the commutation relation between $\hat{V}_I(t_1)$ and $\hat{V}_I(t_2)$ are

$$\left[V_I(t_1), V_I(t_2)\right] = \epsilon^2\cos\omega_d t_1\cos\omega_d t_2\left(2i\sin\omega_R(t_1 - t_2)\right)\hat{I}$$

and

$$\left[\left[V_I(t_1), V_I(t_2)\right], V_I(t_3)\right] = 0.$$

Therefore, given the Campbell-Baker-Hausdorff relation

$$e^{\hat{A}}e^{\hat{B}} = e^{\hat{A}+\hat{B}+\left[\hat{A},\hat{B}\right]/2},$$

$\hat{T}(0,t)$ can be expressed as below.

$$\begin{aligned}\hat{T}(0,t) &= \lim_{\delta\to 0}\hat{T}(0,\delta)\hat{T}(\delta,2\delta)\ldots\hat{T}(t-\delta,t)\\ &= \exp\left\{-\frac{i}{\hbar}\int_0^t \hat{V}_I(t')dt' - \frac{1}{2\hbar^2}\int_0^t dt'\int_0^{t'}\left[V_I(t'), V_I(t'')\right]dt''\right\}\end{aligned}$$

With the rotating wave approximation $\Delta \ll \omega_d + \omega_R$, where $\Delta = \omega_d - \omega_R$, the integrals are evaluated to be

$$-\frac{i}{\hbar}\int_0^t \hat{V}_I(t')dt' \approx \beta\hat{a}^\dagger - \beta^*\hat{a}, \text{ where } \beta = -\frac{i\epsilon \sin \Delta t/2}{\hbar\Delta}e^{i\Delta t/2},$$

and

$$-\frac{1}{2\hbar^2}\int_0^t dt' \int_0^{t'} \left[V_I(t'), V_I(t'')\right] dt'' = iC\left(t\right)\hat{I},,$$

where

$$C\left(t\right) = -\frac{\epsilon^2}{\hbar^2}\int_0^t dt' \int_0^{t'} \cos\omega_d t' \cos\omega_d t'' \sin\omega_R\left(t' - t''\right)dt''$$

Therefore, the first term in Equation A1 gives a displacement operator $\hat{D}(\beta) = e^{\beta\hat{a}^\dagger - \beta^*\hat{a}}$, while the second term only provides an overall time-dependent phase shift. The overall phase shift can be ignored here.

If the initial state is a coherent state $|\alpha\rangle$, then the effect of the time evolution is to displace the coherent state by β with some additional phase shift as shown below.

$$\begin{aligned} |\Psi(t)\rangle &= \hat{T}\left(0,t\right)|\Psi(0)\rangle = \hat{T}\left(0,t\right)|\alpha\rangle \\ &= e^{iC(t)}\hat{D}(\beta)|\alpha\rangle \\ &= e^{iC(t)}e^{iIm\{\alpha\beta^*\}}|\alpha+\beta\rangle \end{aligned} \tag{A1}$$

Back in the Schrodinger picture, the state is expressed as

$$|\psi(t)\rangle = \hat{U}^\dagger|\Psi(t) = e^{-i\omega_R t/2}|\left(\alpha+\beta\right)e^{-i\omega_R t}\rangle.$$

2. Demonstration of Fock state preparation

Similar to what has been demonstrated in Ref. [5], here demonstrates how to prepare Fock state from vacuum with GRAPE algorithm. In the dispersive regime, the drift Hamiltonian is set to $H_{drift} = \chi\hat{a}^\dagger\hat{a}|e\rangle\langle e|$ and the control is $H_{control} = \epsilon_c\hat{a} + \epsilon_T\hat{\sigma}_- + h.c.$. Here, adopt the value $\chi = 2.2$MHz and total time $T = 0.5\mu$s. The initial state is set to $|0,g\rangle$ and the target state to fock state $|6,g\rangle$. The resulting pulse is shown in Figure 6.

With these control pulses, evolving the initial state under Schrodinger's equation to reach the final state, and their Wigner functions are shown in Figure 7. The overlap between the target state and the final state is around 99.5%, thus realizing fock state preparation.

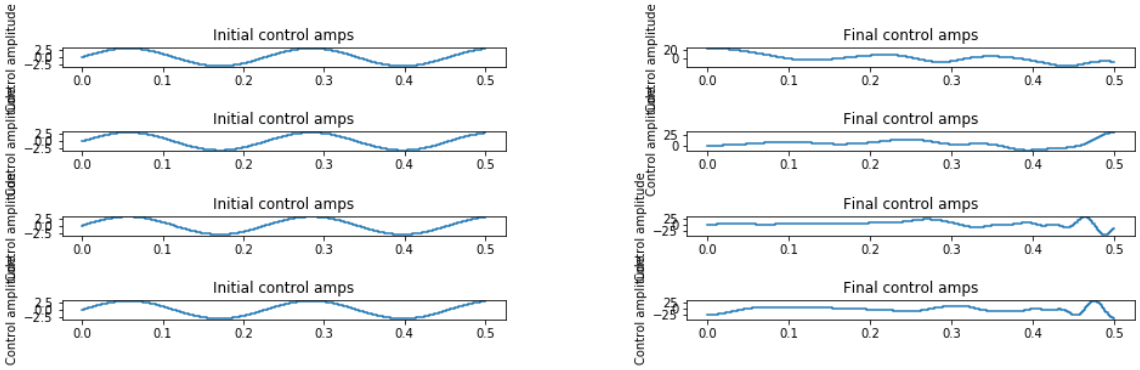

(a) Initial guessed pulse

(b) Final optimized pulse

FIG. 6: Control amplitudes of the 4 control Hamiltonian.

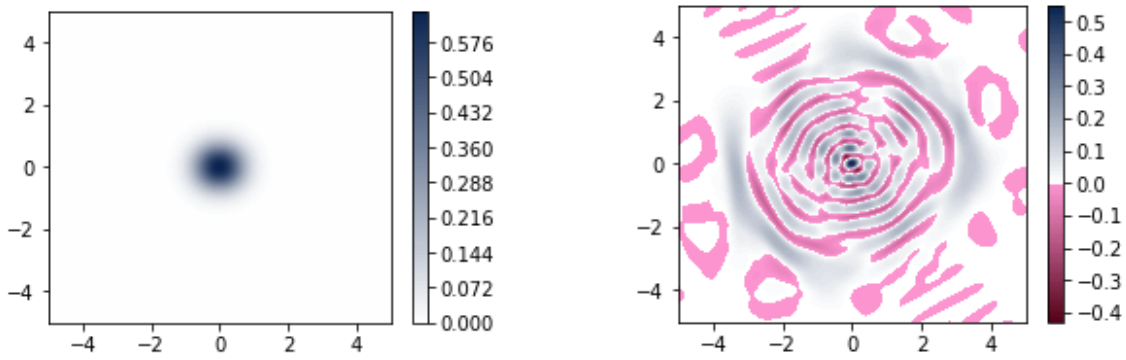

(a) Initial state $|0\rangle|g\rangle$

(b) Final state

FIG. 7: Wigner functions of the initial and final states

Appendix B: Hubbard model

1. Explicit mapping of the Hubbard Hamiltonian

The Hubbard Hamiltonian shown in Section II A needs to be mapped to the cavity levels with encodings specified. Here, an example is given for the mapping of the hopping Hamiltonian of two electrons of the same spin. The hopping Hamiltonian

$$\hat{T} = -t \sum_{i,\sigma} \left(\hat{c}^{\dagger}_{i,\sigma} \hat{c}_{i+1,\sigma} + \hat{c}^{\dagger}_{i+1,\sigma} \hat{c}_{i,\sigma} \right).$$

The commutation relation for fermions operators from second quantization are

$$\left\{\hat{c}_i, \hat{c}_j\right\} = 0,\ \left\{\hat{c}_i^\dagger, \hat{c}_j^\dagger\right\} = 0, \text{ and } \left\{\hat{c}_i^\dagger, \hat{c}_j\right\} = \delta_{i,j}.$$

With the encoding $\begin{pmatrix} \hat{c}_2^\dagger\hat{c}_1^\dagger|0\rangle \\ \hat{c}_4^\dagger\hat{c}_1^\dagger|0\rangle \\ \hat{c}_3^\dagger\hat{c}_1^\dagger|0\rangle \\ \hat{c}_4^\dagger\hat{c}_2^\dagger|0\rangle \\ \hat{c}_3^\dagger\hat{c}_2^\dagger|0\rangle \\ \hat{c}_4^\dagger\hat{c}_3^\dagger|0\rangle \end{pmatrix}$ to the first 6 cavity energy levels, the matrix elements are calculated to be

$$\hat{T} = -t \begin{pmatrix} 0 & 0 & 1 & -1 & 0 & 0 \\ 0 & 0 & 1 & 1 & 0 & 0 \\ 1 & 1 & 0 & 0 & 1 & -1 \\ -1 & 1 & 0 & 0 & 1 & 1 \\ 0 & 0 & 1 & 1 & 0 & 0 \\ 0 & 0 & -1 & 1 & 0 & 0 \end{pmatrix}.$$

Generalized expression for an arbitrary number of spin-up and spin-down electrons can be calculated automatically using libraries such as SymPy or OpenFermion.

2. Ground state of strongly correlated half-filled Hubbard model

The ground state of the half-filled Hubbard model with 2 spin-up and 2 spin-down electrons can be easily obtained to be -4t when U=0. In the case of U/t $\gg$ 1, the ground state can be solved with perturbation theory. It is desirable to find an effective Hamiltonian for the low energy states, i.e. no double occupation. Divide the hopping Hamiltonian into

$$\hat{T} = \hat{T}_0 + \hat{T}_+ + \hat{T}_-$$

such that $\hat{T}_0$ conserves the number of double occupation states, and $\hat{T}_\pm$ increase/decrease the number of double occupation states by one. Here, construct an unitary such that in the rotating frame, the effective Hamiltonian do not have first order $\hat{T}_\pm$, which can lead low energy states to high energy states. Construct the unitary to be $\hat{W} = e^{\hat{S}}$, where $\hat{S} = \lambda(\hat{T}_+ - \hat{T}_-)$. The effective Hamiltonian is then

$$\hat{H}' = \hat{W}\hat{H}\hat{W}^\dagger = \hat{H} + \left[\hat{S}, \hat{H}\right] + \frac{1}{2!}\left[\hat{S}\left[\hat{S}, \hat{H}\right]\right] + \cdots.$$

Considering the definitions of $\hat{T}_{0,\pm1}$, it is straightforward that $\left[\hat{V}, \hat{T}_m\right] = mU\hat{T}_m$, where m takes values 0 and ±1. Then,

$$\begin{aligned}\hat{H}' &= \hat{W}\hat{H}\hat{W}^\dagger \\ &= \hat{H} + \left[\hat{S}, \hat{H}\right] + \frac{1}{2!}\left[\hat{S}\left[\hat{S}, \hat{H}\right]\right] + \cdots \\ &= \hat{V} + \hat{T}_0 + (1 - \lambda U)\left(\hat{T}_+ + \hat{T}_-\right) + \lambda\left(\left[\hat{T}_+ - \hat{T}_-, \hat{T}\right]\right) - \lambda^2 U\left[\hat{T}_+, \hat{T}_-\right] + \mathcal{O}(\lambda^2 t^3) \quad \text{(B1)}\end{aligned}$$

To get rid of the term linear in $\hat{T}_\pm$, let $\lambda = 1/U$. Besides, when in the low energy states, there are no doubly occupied states, therefore $\hat{T}_-$ and $\hat{V}$ always returns 0. If considering half-filled, then $\hat{T}_0$ also gives 0. Since $\hat{T}_0 = \hat{T}_0^\dagger$, the term $\hat{T}_0\hat{T}_+$ also vanishes. The effective Hamiltonian is then only left with

$$\hat{H}' = -\frac{1}{U}\hat{T}_-\hat{T}_+.$$

The possible low energy states with two spin-up and two spin-down electrons are $|\uparrow\uparrow\downarrow\downarrow\rangle$, $|\downarrow\uparrow\uparrow\downarrow\rangle$, $|\downarrow\downarrow\uparrow\uparrow\rangle$, $|\uparrow\downarrow\downarrow\uparrow\rangle$, $|\downarrow\uparrow\downarrow\uparrow\rangle$, and $|\uparrow\downarrow\uparrow\downarrow\rangle$, where the last two are the *Néel* states. In the basis of $\begin{pmatrix} |\uparrow\uparrow\downarrow\downarrow\rangle \\ |\downarrow\uparrow\uparrow\downarrow\rangle \\ |\downarrow\downarrow\uparrow\uparrow\rangle \\ |\uparrow\downarrow\downarrow\uparrow\rangle \\ |\uparrow\downarrow\uparrow\downarrow\rangle \\ |\downarrow\uparrow\downarrow\uparrow\rangle \end{pmatrix}$, the effective Hamiltonian is $-\frac{t^2}{U}\begin{pmatrix} 4 & 0 & 0 & 0 & 2 & 2 \\ 0 & 4 & 0 & 0 & 2 & 2 \\ 0 & 0 & 4 & 0 & 2 & 2 \\ 0 & 0 & 0 & 4 & 2 & 2 \\ 2 & 2 & 2 & 2 & 8 & 0 \\ 2 & 2 & 2 & 2 & 0 & 8 \end{pmatrix}$. The lowest eigenvalue of this matrix gives the ground state energy $E_{ground} = -12\frac{t^2}{U}$ with a corresponding ground state $\frac{1}{2\sqrt{3}}\begin{pmatrix} 1 \\ 1 \\ 1 \\ 1 \\ 2 \\ 2 \end{pmatrix}$.

As a verification, Figure 8 gives the plot of ground state energy in units of U vs the ratio of t/U. In the limit of small t/U, i.e. strongly correlated electrons, the ground state given by diagonalization fits well to the theoretically predicted ground state of $E_{ground} = -12\frac{t^2}{U}$. In the limit of high t/U, as derived before, the ground state energy should tend to -4t, i.e. linear.

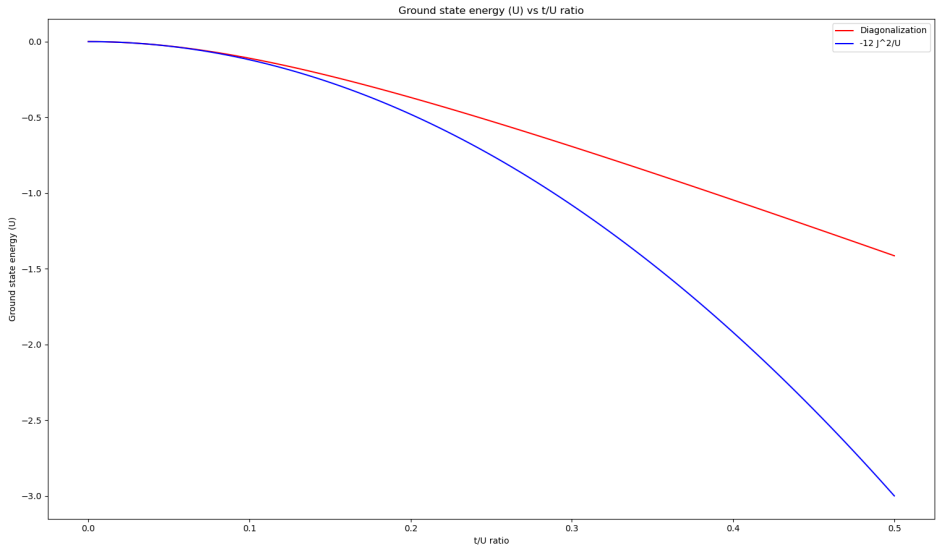

FIG. 8: Comparison of derived ground state energy of half-filled Hubbard model with 4 sites to the ground state energy from diagonalization in the limit of $U/t \gg 1$.

Appendix C: Model selection

1. Control types

There are various controls that can be applied to the cavity-qubit systems. As a summary, the possible types of controls are included in Table I. The label names are adopted in the plot labels.

In order to determine the best performance control type, Figure 9 shows the infidelity trend for each control types. It can be concluded that control types with identical controls on both cavities perform generally better than the ones with individual controls. Within those, symmetric beam splitter control and two-mode squeezer controls perform around equally well individually or combined.

2. GRAPE algorithm

For GRAPE algorithm, there are many hyper-parameters subject to optimization such as the number of time slices and the truncated Hilbert space dimension. An example of paramter choice is given for the dynamics simulation problem.

Controls		
Control terms	Names	Labels
$\left\{\hat{a}_1+\hat{a}_1^\dagger, i\left(\hat{a}_1-\hat{a}_1^\dagger\right), \sigma_{1,x}, \sigma_{1,y}\right\}, \left\{\hat{a}_2+\hat{a}_2^\dagger, i\left(\hat{a}_2-\hat{a}_2^\dagger\right), \sigma_{2,x}, \sigma_{2,y}\right\}$	Independent controls	independent
$\left(\hat{a}_1+\hat{a}_1^\dagger+\hat{a}_2+\hat{a}_2^\dagger\right)$, $i\left(\hat{a}_2-\hat{a}_2^\dagger\right) + i\left(\hat{a}_1-\hat{a}_1^\dagger\right)$, $\left(\sigma_{1,x}+\sigma_{2,x}\right)$, $\left(\sigma_{1,y}+\sigma_{2,y}\right)$.	Identical controls	identical
$\left\{\hat{a}_1^\dagger\hat{a}_2+\hat{a}_1\hat{a}_2^\dagger, i\left(\hat{a}_1^\dagger\hat{a}_2-\hat{a}_1\hat{a}_2^\dagger\right)\right\}$	Beam splitter	bs
$\left\{\hat{a}_1^\dagger\hat{a}_2+\hat{a}_1\hat{a}_2^\dagger\right\}$	Beam splitter with symmtry	symbs
$\left\{\hat{a}_1^\dagger\hat{a}_2^\dagger+\hat{a}_1\hat{a}_2, i\left(\hat{a}_1^\dagger\hat{a}_2^\dagger-\hat{a}_1\hat{a}_2\right)\right\}$	Mode squeezer	sq
No interaction controls between cavities		noInt
No individual controls on the cavities		noCav

TABLE I: Summary of available control types.

With a single cavity, Figure 10 shows the infidelity vs the truncated Hilbert space dimension and infidelity vs number of time slices. It is observed that when dominated by hopping Hamiltonian, there should be $N_{cav} = 10$ and $N_{ts} = 40$ for cavities simulating 1 spin-up electron and $N_{cav} = 16$ and $N_{ts} = 60$ for cavities simulating 2 spin-up electrons.

Similar plots can be shown for variational method, and the results suggests there should be $N_{cav} = 8$ and $N_{ts} = 40$ for cavities simulating 1 spin-up electron and $N_{cav} = 10$ and $N_{ts} = 60$ for cavities simulating 2 spin-up electrons.

Appendix D: GRAPE algorithm modifications

1. QuTip implementation details

Assume the truncated Hilbert space to have dimension N_{cavity}, the total time slice number to be n, and the duration of each time slice is Δt. In general, the Hamiltonian can be expressed as

$$\hat{H}\left(t_i\right) = \hat{H}_{drift}\left(t_i\right) + \sum_j \epsilon_j\left(t_i\right)\hat{H}_j$$

, where ϵ_i is the control pulse amplitude subject to optimization. The pulse amplitude ϵ_i is constant in each time slice t_i to $t_i + \Delta t$.

Here discuss the case when the target is an unitary operator, but it can be easily generalized to include target state. Assume the target operator is $\hat{U}_{targ}$. Assume the

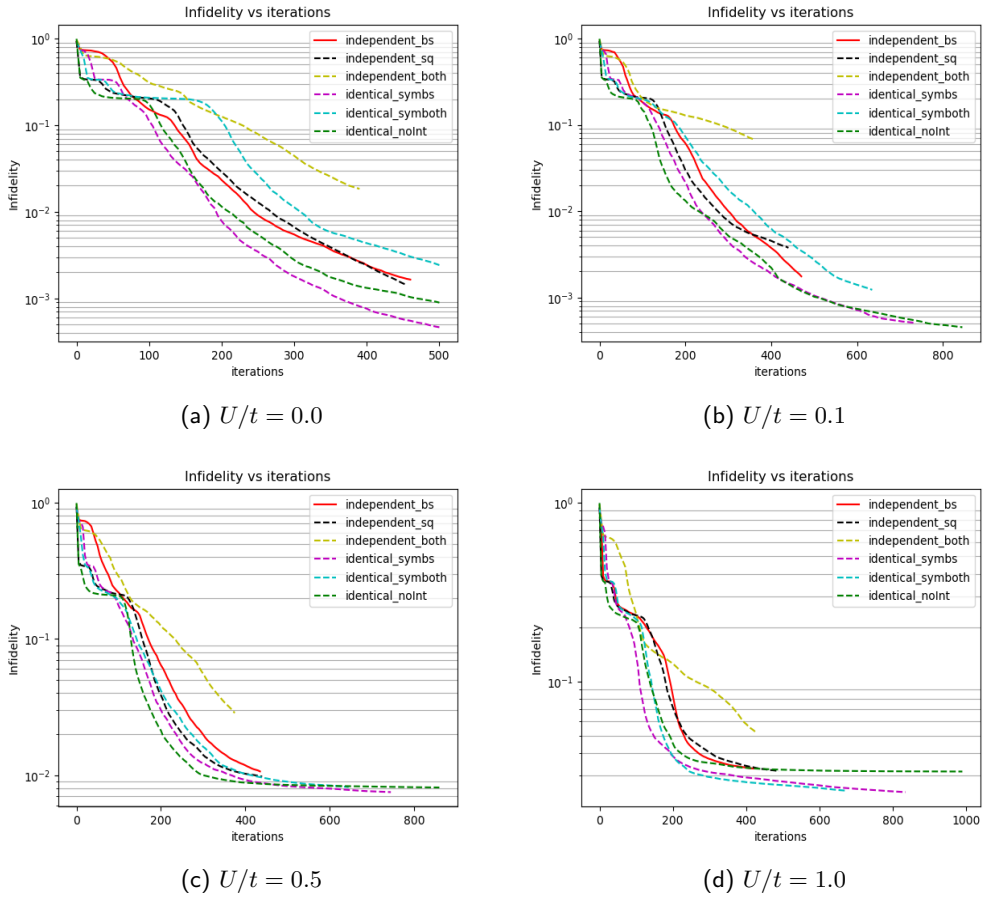

(a) $U/t = 0.0$ (b) $U/t = 0.1$

(c) $U/t = 0.5$ (d) $U/t = 1.0$

FIG. 9: Infidelity of dynamics simulation for [1,1] vs GRAPE iterations for all combinations of control types under different U/t ratios.

propagator for time slice i be $\hat{A}_i$, where i range from 1 to n. The initial operator is $\hat{U}_0$, which is usually set to the identity operator. The resulting operator from the Hamiltonian is

$$\hat{U}_f = \hat{A}_n \cdots \hat{A}_2 \hat{A}_1 \hat{U}_0$$

. $\hat{A}_i$ is calculated through decomposition. Let the eigen-basis decomposition of the total Hamiltonian be

$$\hat{H}(t_i) = \hat{V}\hat{D}\hat{V}^\dagger, \text{ where } \hat{V} = \begin{bmatrix} \vec{v}_1 & \vec{v}_2 & \cdots & \vec{v}_N \end{bmatrix} \text{ and } \hat{D} = \begin{bmatrix} \lambda_1 & & \\ & \ddots & \\ & & \lambda_N \end{bmatrix}$$

. Then, the propagator $\hat{A}_i = e^{-i\Delta t\hat{H}(t_i)} = \hat{V}e^{-i\Delta tD}\hat{V}^\dagger$.

The default fidelity expression in QuTip for unitary evolution is the Hilbert-Schmidt inner product

$$f_{HS} = \frac{Tr\left\{\hat{U}_{targ}^{-1}\hat{U}_f\right\}}{N} = |f_{HS}|e^{i\theta}$$

. When global phase is ignored, the fidelity is taken to be $f = |f_{HS}|$, which range from 0 to 1 when it's unitary evolution. The derivative can be calculated as

$$\frac{\partial f}{\partial \epsilon_i} = \frac{\partial\sqrt{f_{HS}^* f_{HS}}}{\partial\epsilon_i} = \frac{1}{2}\,\mathrm{Re}\left\{\frac{e^{-i\theta}}{N}\frac{\partial Tr\left\{\hat{U}_{targ}^{-1}\hat{U}_f\right\}}{\partial\epsilon_i}\right\} = \frac{1}{2}\,\mathrm{Re}\left\{\frac{e^{-i\theta}}{N}Tr\left\{\hat{U}_{targ}^{-1}\hat{A}_n\cdots\frac{\partial\hat{A}_i}{\partial\epsilon_i}\cdots\hat{A}_1\hat{U}_0\right\}\right\},$$

and the propagator gradient is then calculated as

$$\frac{\partial\hat{A}_i}{\partial\epsilon_i} = \frac{\partial\left(\hat{V}e^{-i\Delta tD}\hat{V}^\dagger\right)}{\partial\epsilon_i} = \hat{V}\hat{B}\hat{V}^\dagger,$$

where

$$\hat{B} = \hat{V}^\dagger\frac{\partial\hat{V}}{\partial\epsilon_i}e^{-i\Delta tD} + \frac{\partial e^{-i\Delta tD}}{\partial\epsilon_i} + e^{-i\Delta tD}\frac{\partial\hat{V}^\dagger}{\partial\epsilon_i}\hat{V}$$

Applying perturbation theory to the eigenvalues and eigenvectors, the expression turns to

$$B_{l,m} = \left(1-\delta_{l,m}\right)\left(e^{-i\Delta t\lambda_l} - e^{-i\Delta t\lambda_m}\right)\frac{\vec{v_l}^\dagger\hat{H}_i\vec{v_m}}{\lambda_l-\lambda_m} + \delta_{l,m}\left(-i\Delta t\right)e^{-i\Delta t\lambda_l}\left(\vec{v_l}^\dagger\hat{H}_i\vec{v_l}^\dagger\right).$$

Expressing with the conventions set in QuTip, $B_{l,m} = Q_{l,m}W_{l,m}$, i.e. it's the element-wise product of W and Q, where $\hat{W} = \hat{V}^\dagger\hat{H}_i\hat{V}$ and $Q_{l,m} = \left(1-\delta_{l,m}\right)\frac{e^{-i\Delta t\lambda_l}-e^{-i\Delta t\lambda_m}}{\lambda_l-\lambda_m} + \delta_{l,m}\left(-i\Delta t\right)e^{-i\Delta t\lambda_l}$.

2. Modifications

a. Customized fidelity expression

For dynamics simulation, the expression for fidelity is modified to be

$$f = \frac{\left|Tr\left\{\hat{I}_{N_{dim},gg}\left(\hat{U}_{targ}^{-1}\hat{U}_f\right)\right\}\right|}{N_{dim}},\ \text{where}\ \hat{I}_{N_{dim},gg} = \left[\begin{array}{c|c}\hat{I} & \\ \hline & \mathbf{0}\end{array}\right]|g\rangle\langle g|$$

Not here $\left[\begin{array}{c|c} \hat{I} & \\ \hline & \mathbf{0} \end{array}\right]$ is a $N_{cav} \times N_{cav}$ matrix with the identity matrix $\hat{I}$ of size $N_{dim} \times N_{dim}$. The derivative is then easily generalized to be

$$\frac{\partial f}{\partial \epsilon_i} = \frac{1}{2}\,\mathrm{Re}\left\{\frac{e^{-i\theta}}{N} Tr\left\{\hat{I}_{N_{dim},gg}\hat{U}_{targ}^{-1}\hat{A}_n \cdots \frac{\partial \hat{A}_i}{\partial \epsilon_i} \cdots \hat{A}_1\hat{U}_0\right\}\right\},$$

For variational methods, the cost function to minimize is then

$$\mathrm{cost} = \langle\Psi|\hat{H}|\Psi\rangle = \langle i|\hat{U}_f^\dagger \hat{H}\hat{U}_f|i\rangle,$$

and the gradients

$$\frac{\partial \mathrm{cost}}{\partial \epsilon_i} = 2\,\mathrm{Re}\left\{\langle i|\hat{U}_f^\dagger \hat{H}\hat{A}_n \cdots \frac{\partial \hat{A}_i}{\partial \epsilon_i} \cdots \hat{A}_1|i\rangle\right\}.$$

Note that in both cases, the propagator gradients $\frac{\partial \hat{U}_i}{\partial \epsilon_i}$ have the same expressions as outlined in the previous section.

b. Arbitrary input initial pulse shapes

We have modified the source code of QuTip such that the input pulse can be self-defined. In QuTip's original implementation, the initial pulse guess can only be one of a few types such as random and Sinusoidal. However, having the flexibility to input arbitrary pulse is critical to some methods such as adiabatically turning up the Hamiltonian during the optimization. This issue is also addressed in a recent Krotov's implementation documentions [8].

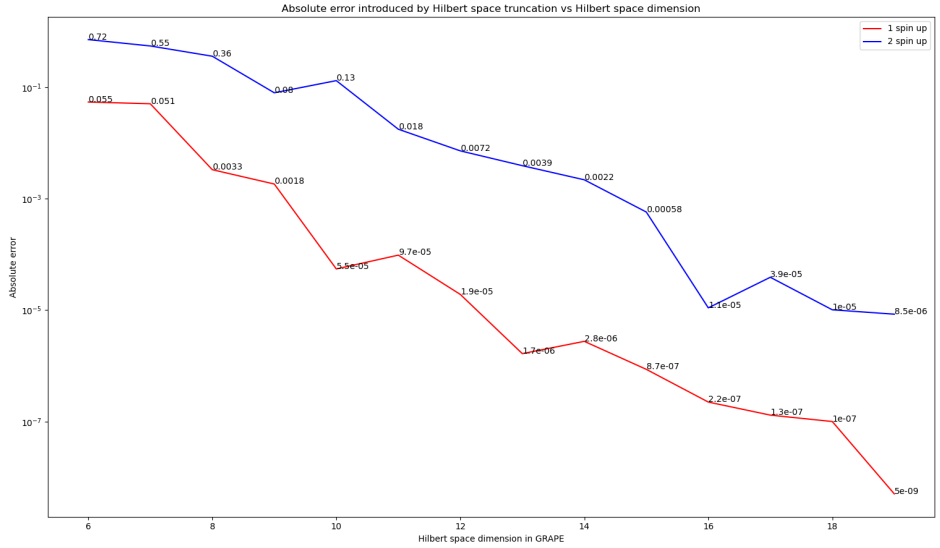

(a) Absolute error in infidelity vs dimension of truncated Hilbert space

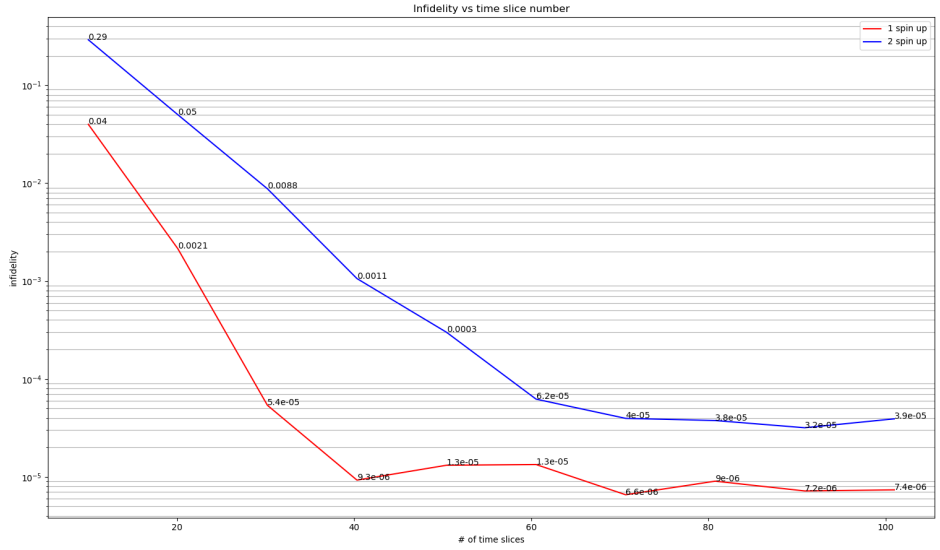

(b) Infidelity of dynamics simulation vs number of time slices.

FIG. 10: Parameters choice for dynamics simulation. Results are shown for both 1 and 2 spin-up electrons.